Large-eddy simulation of kerosene spray combustion in a model scramjet chamber

M Zhang[1]*, **Z Hu**[2], **G He**[1], and **P Liu**[1]

[1]National Key Laboratory of Combustion, Flow and Thermo-Structure, Northwestern Polytechnical University, Xi'an, People's Republic of China

[2]Aerodynamics and Flight Mechanics Research Group, School of Engineering Sciences, University of Southampton, Southampton, UK

The manuscript was received on 31 October 2009 and was accepted after revision for publication on 18 January 2010.

DOI: 10.1243/09544100JAERO738

Abstract: Large-eddy simulation (LES) of kerosene spray combustion in a model supersonic combustor with cavity flame holder is carried out. Kerosene is injected through the ceiling of the cavity. The subgrid-scale (SGS) turbulence stress tensor is closed via the Smagorinsky's eddy-viscosity model, chemical source terms are modelled by a finite rate chemistry (FRC) model, and a four-step reduced kerosene combustion kinetic mechanism is adopted. The chamber wall pressure predicted from the LES is validated by experimental data reported in literature. The test case has a cavity length of 77 mm and a depth of 8 mm. After liquid kerosene is injected through the orifice, most of the droplets are loaded with recirculation fluid momentum inside the cavity. Due to lower velocity of the carrier fluid inside the cavity, sufficient atomization and evaporation take place during the process of droplet transportation, resulting in a rich fuel mixture of kerosene vapour accumulating inside the cavity. These rich fuel mixtures are mixed with fresh air by the approach mixing layer at the front of the cavity and are thus involved in burning accompanied with the approach boundary layer separation extending towards upstream. The combustion flame in the downstream impinges onto the rear wall of the cavity and is then reflected back to the front of the cavity. During the recirculation of hot flow, heat is compensated for evaporation of droplets. The circulation processes mentioned above provide an efficient flame-holding mechanism to stabilize the flame. Comparisons with results from a shorter length of cavity (cavity length of 45 mm) show that, due to insufficient atomization and evaporation of the droplets in the short distance inside the cavity, parts of the droplets are carried out of the cavity through the boundary layer fluctuation and evaporated in the hot flame layer, thus resulting in incomplete air fuel mixing and worse combustion performance. The flow structures inside the cavity play an important role in the spray distribution, thus determining the combustion performance.

Q1

1 INTRODUCTION

Technology to organize supersonic combustion is critical for the next generation of high-speed aircrafts such as ramjet, dual-mode ramjet/scramjet, and other kinds of ramjet-based combined engines [**1**–**4**]. A previous study [**5**] showed that liquid hydrocarbon fuels presented a viable alternative to gaseous hydrogen in terms of energy density and handling issues for flight Mach numbers below 9. However, during the hydrocarbon fuel combustion, liquid fuels must undergo a series of processes including the primary breakup (nozzle atomization), the aerodynamic-induced liquid sheet atomization, and the mass transfer accompanied with heat exchange around liquid droplets between the liquid and the vapour phase [**6**, **7**]. These physical phenomena cover a broad range of research topics such as turbulence, multiphase flow, multi-component flow, combustion, and their interactions [**6**–**10**]. Any subjects mentioned here need profound and systematic knowledge, which hinder the process of crossing the threshold of a better

*Corresponding author: National Key Laboratory of Combustion, Flow and Thermo-Structure, Northwestern Polytechnical University, Xi'an 710072, People's Republic of China.
email: zm2001er@yahoo.com.cn

understanding of spray combustion. Additionally, due to high-speed and high-temperature operating conditions in supersonic spray combustion, experimental investigations are short to get sufficient details of combustion flow structures.

Developments in computational fluid dynamic (CFD) techniques and supercomputers have enabled more complicated engineering cases to be studied by performing numerical simulations. In the past decades, time-averaged solution of the Reynolds-averaged Navier–Stokes (RANS) equations was routinely used in the fluid dynamics and combustion study and shown reasonable prediction accuracy [**11**–**13**]. With this tool, only the mean quantities are available, and all the effects of turbulence on the mean field are modelled. However, Baurle [**14**], focused on high-speed turbulent reacting flow, demonstrated that the simple species diffusion models in RANS have proved to be evidently troublesome. Species diffusion and mixing processes are dominated by the solution of turbulent flow due to the strong impact of turbulence. Hence, more accurate turbulence simulation is a prerequisite to obtain better description of turbulent reaction especially for simulations to obtain combustion flame structures, which is not satisfied with just the mean flow solutions [**15**–**17**].

In recent years, time-accurate approaches, such as large-eddy simulation (LES) and detached-eddy simulation, gradually move from pure research cases to practical applications. LES can offer access to a spatially and temporally dependent flow description. More importantly, the transient physical information of the complex fluid flow cannot be obtained from RANS. This advanced numerical method opens a new perspective into turbulence research, especially for turbulent combustion where transient physical phenomena are known to be critical [**9**, **15**–**19**].

From recent publications, which are mainly referred to the works about spray combustion simulations [**20**–**23**], it can be seen that LES studies conducted by Pael and Menon [**20**], Pael *et al.* [**21**, **22**], and Genin and Menon [**23**] in Georgia Institute of Technology have been applied to real combustors. Pael and Menon [**20**–**22**] carried out a two-phase reacting LES in a gas turbine chamber. In their work, LES turbulence–combustion interaction is modelled via linear eddy model, the spray analysis is based on a Lagrangian droplet model which includes empirical evaporation and secondary breakup model, and the reaction is modelled with a global multi-step mechanism. Some unsteady flow features such as vortex breakdown and shear layer mixing are identified form LES data, which give an in-depth understanding of spray dispersion, fuel–air mixing, and flame stabilization. Genin and Menon [**23**] conducted LES of spray combustion in a supersonic ramjet chamber. Due to the high speed in the combustor, reaction rate is considered to be controlled by turbulence timescale, thus it is modelled via the subgrid eddy break-up model. As a result, some flow characteristics such as the shear layer mixing properties are obtained from their LES study.

In fact, although the application of LES of turbulent spray combustion for both gas turbine chambers and ramjet combustors have seen some successes in recent years, the LES study of spray combustion for industry applications still need further development. With regard to the supersonic transport vehicle development mentioned at the start of this article, deep understanding of supersonic spray combustion is necessary. However, until recently, study in the related topics has little been reported in open literatures. Thus, the mechanism of supersonic spray combustion is still an outstanding issue and needs further investigation as it has strong implication on the combustor performance.

To achieve better understanding on kerosene spray combustion under supersonic flow conditions, LES of kerosene spray combustion in a model ramjet chamber is conducted in this paper. Results are compared with experimental data with good agreement. The analysis of droplets, the time-averaged results of reaction flow structure, and the transient flow details are given as the attempt to reveal reaction flow mechanism. Considering the open questions related to LES applications [**24**], such as the turbulence–combustion interaction [**9**, **25**–**31**], the chemical kinetic mechanism [**32**], and the droplet evaporation and atomization [**33**], details of methodology about some open issues are also discussed in this paper.

2 METHODOLOGY

2.1 Governing equations for the gaseous phase

Gaseous phase is controlled by Navier–Stokes equations coupled with reaction source and dispersed phase source, which are filtered through Favre average method, and can be written in tensor notation as

$$\frac{\partial \bar{\rho}}{\partial t} + \frac{\partial}{\partial x_j}(\bar{\rho}\tilde{u}_j) = \tilde{S}_m \tag{1}$$

$$\frac{\partial}{\partial t}(\bar{\rho}\tilde{u}_i) + \frac{\partial}{\partial x_j}(\bar{\rho}\tilde{u}_i\tilde{u}_j) = \frac{\partial}{\partial x_j}(-\delta_{ij}\bar{P} + \tilde{\tau}_{ij} - \tau^{\mathrm{sgs}}) + \tilde{S}_{ui} \tag{2}$$

$$\frac{\partial}{\partial t}(\bar{\rho}\tilde{h} - \bar{P}) + \frac{\partial}{\partial x_j}(\bar{\rho}\tilde{h}\tilde{u}_j + h_j^{\mathrm{sgs}}) = \frac{\partial}{\partial x_j}(-\tilde{q}_j + \tilde{\tau}_{ij}\tilde{u}_i - \sigma_j^{\mathrm{sgs}}) + \tilde{S}_h \tag{3}$$

$$\frac{\partial}{\partial t}(\bar{\rho}\tilde{Y}_m) + \frac{\partial}{\partial x_j}[\bar{\rho}\tilde{Y}_m\tilde{u}_j - \bar{\rho}\tilde{Y}_m\tilde{V}_{j,m} + Y_{j,m}^{\mathrm{sgs}} + \theta_{j,m}^{\mathrm{sgs}}] = \tilde{S}_{Y_m} + \tilde{\dot{\omega}}_m \tag{4}$$

Equations (1) to (3) are the conservative laws for mass, momentum, and energy, respectively.

Equation (4) is the multi-component transportation equation. In the above equations, the source term $\tilde{S}_m$ stands for mass transfer between the gaseous phase and the liquid phase caused by spray evaporation, $\tilde{S}_{ui}$ stands for the momentum interaction between the gaseous phase and the liquid phase, $\tilde{S}_h$ stands for the energy transfer between the gaseous phase and the liquid phase, $\tilde{S}_{Y_m}$ is the mass transfer for species m, and $\tilde{\dot{\omega}}_m$ is the species production rate.

According to the constitutive equation of Newton fluid, $\tilde{\tau}_{ij}$ in equation (2) can be given by

$$\tilde{\tau}_{ij} = \mu\left[\left(\frac{\partial \tilde{u}_i}{\mathrm{dx_j}} + \frac{\partial \tilde{u}_j}{\mathrm{dx_i}}\right) - \frac{2}{3}\delta_{ij}\frac{\partial \tilde{u}_k}{\mathrm{dx_k}}\right] \tag{5}$$

where μ is the molecular viscosity that varies with temperature according to the Sutherland law. δ_{ij} is the Kronecker delta function. τ^{sgs} is the subgrid-scale (SGS) stress tensor, which is modelled in LES. In this work, τ^{sgs} is modelled via Bousinesq assumption and is expressed as

$$\tau^{\mathrm{sgs}} = -2\nu_{\mathrm{t}}\tilde{S}_{ij} + \frac{1}{3}\delta_{ij}\tau_{kk} \tag{6}$$

where ν_{t} is the SGS viscosity given by Smagorinsky's eddy-viscosity model

$$\nu_{\mathrm{t}} = (C_{\mathrm{s}}\Delta)^2(2\tilde{S}_{ij}\tilde{S}_{ij})^{1/2} \tag{7}$$

Here Δ is the filter width and C_{s} is the Smagorinsky constant, chosen to be 0.1 in this study.

In equation (3), $\tilde{h}$ is the resolved chemical enthalpy and $\tilde{q}_j$ is the resolved heat flux vector. For multi-species flow, $\tilde{q}_j$ can be decomposed into heat conduction, energy flux due to inter-species diffusion, and SGS heat flux, as

$$\tilde{q}_j = -\bar{\lambda}\frac{\partial \tilde{T}}{\partial x_j} + \sum_{m=1}^{Ns}\bar{\rho}\tilde{Y}_m\tilde{V}_{j,m}\tilde{h}_m + \sum_{m=1}^{Ns}q_{j,m}^{\mathrm{sgs}} \tag{8}$$

where $\bar{\lambda}$ is the thermal conductivity, $\tilde{Y}_m$ and $\tilde{V}_{j,m}$ are the mass fraction and diffusion velocity of species m, respectively, and $q_{j,m}^{\mathrm{sgs}}$ is the SGS heat flux. The diffusion velocity $\tilde{V}_{j,m}$ is approximated using Fick's law of diffusion and can be written as

$$\tilde{V}_{j,m} = -\frac{\tilde{D}_m}{\tilde{Y}_m}\frac{\partial \tilde{Y}_m}{\partial x_j} \tag{9}$$

where $\tilde{D}_m$ is the mass diffusivity of species m relative to the mixture.

Additionally, h_j^{sgs} is the SGS enthalpy flux, σ_j^{sgs} is the SGS viscous term, $Y_{j,m}^{\mathrm{sgs}}$ is the SGS convective species flux, and $\theta_{j,m}^{\mathrm{sgs}}$ is the SGS species diffusive flux. In most LES approach, the models of h_j^{sgs} and $Y_{j,m}^{\mathrm{sgs}}$ are usually based on the assumption of eddy viscosity, thus these two terms can be written as

$$h^{\mathrm{sgs}} = -\bar{\rho}\frac{\nu_{\mathrm{t}}}{Pr_{\mathrm{t}}}\frac{\partial \tilde{h}}{\partial x_j} \tag{10}$$

$$Y_{j,m}^{\mathrm{sgs}} = -\bar{\rho}\frac{\nu_{\mathrm{t}}}{Sc_{\mathrm{t}}}\frac{\partial \tilde{Y}_m}{\partial x_j} \tag{11}$$

Here Pr_{t} and Sc_{t} are turbulent Prandtl number and Schmidt number, respectively. The other SGS terms σ_j^{sgs}, $\theta_{j,m}^{\mathrm{sgs}}$, and $q_{j,m}^{\mathrm{sgs}}$ are neglected.

However, there is still a critical term left $\tilde{\dot{\omega}}_m$, which governs the whole processes of reaction and must be treated carefully. This issue will be discussed later.

2.2 Governing equations for the dispersed phase

The spray field simulated here is assumed to be dilute and is thus modelled through the Lagrangian–Euler approach. The governing equations for droplets are the kinematic, momentum, and heat-transfer equations, and can be written as

$$\frac{\mathrm{d}x_{\mathrm{p},i}}{\mathrm{d}t} = u_{\mathrm{p},i} \tag{12}$$

$$m_{\mathrm{p}}\frac{\mathrm{d}u_{\mathrm{p},i}}{\mathrm{d}t} = \frac{1}{2}C_{\mathrm{D}}\rho_{\mathrm{f}}A_{\mathrm{p}}|U_{\mathrm{S}}|U_{\mathrm{S}} \tag{13}$$

$$(m_{\mathrm{p}}C_{\mathrm{p,d}})\frac{\mathrm{d}T}{\mathrm{d}t} = Q_{\mathrm{C}} + Q_{\mathrm{M}} \tag{14}$$

Here $u_{\mathrm{p},i}$ is the ith component of the droplet velocity, C_{D} is the drag coefficient, ρ_{f} is the carrier phase density, A_{p} is the effective droplet cross-section in fluid, U_{S} is the slip velocity between the fluid and the droplet, Q_{c} is the droplet convective heat transfer, and Q_{M} is the heat transfer induced by mass transfer. C_{D} is given by [**34**]

$$C_{\mathrm{D}} = \begin{cases} \dfrac{24}{Re_{\mathrm{p}}}(1 + 0.15\,Re_{\mathrm{p}}^{0.687}), & Re_{\mathrm{p}} < 1000 \\ 0.44, & Re_{\mathrm{p}} \geqslant 1000 \end{cases} \tag{15}$$

where Re_{p}, the particle Reynolds number, can be expressed as

$$Re_{\mathrm{p}} = \frac{d_{\mathrm{p}}|U_{\mathrm{S}}|}{\mu/\rho_{\mathrm{f}}} \tag{16}$$

Q_{C} and Q_{M} can be obtained from

$$Q_{\mathrm{C}} = \pi d_{\mathrm{p}}\lambda_{\mathrm{f}}Nu(T_{\mathrm{f}} - T_{\mathrm{p}}) \tag{17}$$

$$Q_{\mathrm{M}} = \sum\frac{\mathrm{d}m_{\mathrm{p}}}{\mathrm{d}t}L_{\mathrm{V}} \tag{18}$$

where L_{V} is the latent heat of vaporization that is obtained directly from the liquid property. The Nusselt number Nu is given by [**35**]

$$Nu = 2 + 0.6Re_{\mathrm{p}}^{1/2}Pr_{\mathrm{f}}^{1/3} \tag{19}$$

2.3 Discussion and approach to some open questions

2.3.1 *Turbulence–combustion interaction*

According to the energy cascade theory, turbulent kinetic energy is generated by the largest scales of fluid motion, is transferred to smaller and smaller eddies, and is finally dissipated by viscosity [**36**]. As for the LES of non-reacting flow, only turbulent scales larger than the gird size are resolved directly, and smaller scales are described by SGS models [**37**]. Through many years of development, SGS models have become quite successful in predicting the fluid performance due to the very little turbulence energy contained there. However, when dealing with reacting flows, this situation is totally changed because macroscopic motion is affected by the additional heat and energy release during the processes of combustion which usually happens in the tiny spatial regime (even smaller than the SGS scale) [**16**]. In turn, combustion is also influenced by the turbulence-induced microscopic species diffusion and mixing throughout all scales in the energy cascade. For reaction processes, turbulence and combustion interact across all scales ranging from macroscopic motions to microscopic motions.

In recent years, many chemical models considering turbulence and combustion interaction have been developed [**25–31**]. These models can be divided roughly into two categories, namely flamelet models and FRC models, according to the time scales of turbulence and the reaction rates which dominate the combustion processes. Fureby [**29**] found that FRC models that can handle the chemical processes in different combustion regimes including premixed and non-premixed combustion have more potential application prospects in industry. However, some mathematical difficulties arise in applying FRC models. From a mathematical point of view, the processes of reaction are controlled by the highly non-linear relationship between temperature and various species concentrations as the form of $\dot{\omega}_m = \widetilde{f(\rho, Y_m, T)}$. However, the filtered function of $\widetilde{\dot{\omega}_m} = f(\rho, Y_m, T)$ is hard to be expressed using other resolved scalar terms [**9**], and new SGS terms will arise during the filtering, which stand for the SGS turbulence–combustion interaction.

Q2 One simple approach, called as the quasi-laminar chemistry model, is neglecting the SGS turbulence–combustion terms such as the form of $\widetilde{\dot{\omega}_m} \approx f(\bar{\rho}, \widetilde{Y_m}, \tilde{T})$, which means the resolved turbulence–combustion interaction is considered but SGS interaction is neglected. Recent numerical studies conducted by Fureby [**29**], Norris and Edwards [**30**], and Sun *et al.* [**31**] compare the quasi-laminar chemistry prediction with experimental data. The predicted results of LES with quasi-laminar chemistry model have seen some reasonable accuracy with sufficient computational grid resolution in the results by Fureby [**29**] and Sun *et al.* [**31**]. It is thought that the solution accuracy seems to be more dependent on grid resolution than the modelling of turbulence–chemistry interaction. Therefore, quasi-laminar chemistry model is used in this paper. However, in order to achieve better prediction, LES study with a massive computational grid is used and validated by experimental data for the highly refined combustion characteristics overlaid with large-eddy motions of unstable reaction flow.

2.3.2 *Chemical kinetic mechanism*

Another open question needed to consider carefully is how to choose properly the chemical kinetic models for combustion simulation. As everyone knows, the combustion of hydrocarbon usually involves thousands of chemical compounds and hundreds of chemical steps [**32**]. Until now, developing a comprehensive model that would directly predict in detail the behaviour of any combustion system involving in CFD is still far beyond today's technologies. One realistic approach is semi-kinetic models based on several reactions designed to reproduce the overall behaviour of combustion or stoichiometric models which just contain several basic reaction mechanisms such that the observed major product distribution is accounted for [**38–40**]. The reduced chemistry model seems like the best economical approach to complex turbulent flow simulation. However, it must be clearly known that any reduced chemical model has a very restricted range of conditions. Q2

One realistic model for combustion of hydrocarbon fuel proposed by Hautman *et al.* [**40**] is adopted in this work. This approach can be described by the following basic four irreversible reaction steps.

1. Transformation of the starting hydrocarbon fuel into smaller intermediate hydrocarbons. This step stands for the decomposition of the hydrocarbon fuel.
2. The oxidation of intermediates to CO and H_2.
3. The oxidation of CO to CO_2.
4. Oxidation of H_2 to H_2O.

The original mechanism of this model had been obtained from the experimental results of C_3H_8 in a flow reactor [**40**] and was extended to the more general C_nH_m combustion system [**41**]. This mechanism was evaluated by extensive comparisons of experimental and numerical results [**40–42**] and was proved to show reasonable accuracy in a relatively broader range. In this work, kerosene is modelled as $C_{11}H_{23}$ [**43**], and C_2H_4 is used to represent the combination of all intermediate hydrocarbon components of kerosene decomposition. The original chemistry scheme proposed by Hautman *et al.* [**40**] is listed in Table 1. The comparisons of numerical prediction with experimental results will be given in the following section.

Table 1 Chemistry model for kerosene oxidation with air [**40**]

Reaction	Reaction scheme
(1) $C_nH_m \rightarrow \frac{n}{2}C_2H_4 + \left(\frac{m}{2} - n\right)H_2$	$\omega_1 = 2.09 \times 10^{17} \exp\left(\frac{-24\,962}{T}\right)[C_nH_m]^{0.5}[O_2]^{1.07}[C_2H_4]^{0.4}$
(2) $C_2H_4 + O_2 \rightarrow 2CO + 2H_2$	$\omega_2 = 5.01 \times 10^{14} \exp\left(\frac{-25\,164}{T}\right)[C_2H_4]^{0.9}[O_2]^{1.18}[C_nH_m]^{-0.37}$
(3) $H_2 + \frac{1}{2}O_2 \rightarrow H_2O$	$\omega_3 = 3.31 \times 10^{13} \exp\left(\frac{-20\,634}{T}\right)[H_2]^{0.85}[O_2]^{1.42}[C_2H_4]^{-0.56}$
(4) $CO + \frac{1}{2}O_2 \rightarrow CO_2$	$\omega_4 = 4.00 \times 10^{14} \exp\left(\frac{-20\,131}{T}\right)[CO]^{1.0}[H_2O]^{0.5}[O_2]^{0.25}$

Units are moles, seconds, centimetres, and Kelvin.

2.3.3 Atomization model

With regard to spray flame, the atomization characteristics of spray clusters play a crucial role in determining the combustion performance [**33**, **44**, **45**]. Both over-prediction and under-prediction of droplet atomization would induce an erroneous delay of gaseous combustion. Unfortunately, the physical processes involved in atomization are not yet sufficiently well understood due to the extremely complicated mechanisms. However, several important contributions to the development for the atomization modelling have been made recently [**33**, **46**]. Raju [**47**] compared different empirical atomization models and showed that the empirical atomization models seem to be modest for some spray cases. The empirical atomization model is still being used in a wide range of applications [**20–22**, **48**]. In this paper, the breakup model by Tanner [**49**], which is more applicable to the high-pressure diesel engine, is used for the modelling of the droplet atomization processes.

3 NUMERICAL IMPLEMENTATION

LES has been performed using the software package Ansys-CFX 11.0 on a super parallel computing platform in the University of Southampton. The governing equations are discretized by a finite-volume approach with a second-order central differencing scheme. The half-cone angle for spray injection is chosen to be 5° according to a similar test case of cavity floor injection conducted by Yu *et al.* [**50**]. The injection mass, injection direction, initial temperature, and the orifice area are given as inlet condition. The initial droplet diameter is calculated, assuming that the nozzle is full of liquid. Atomization processes induced by aerodynamics are modelled by the ETAB breakup model [**49**]. Fully supersonic condition is imposed at the inflow by specifying the mean flow velocity, temperature, and pressure, which are obtained from a separate LES of channel flow. Perturbation is added to the stream-wise velocity component. It is a sinusoidal wave with a frequency of 50 kHz, and the amplitude is decided to give an inlet turbulence intensity of 5 per cent. The combustion chamber wall, where the cavity flame-holder is fitted, is assumed to be impermeable, no-slip, whereas the other side is assumed to be symmetric. Close to the wall, turbulent viscosity is damped by the law of Van Driest damping function [**12**], and the damping factor is chosen as 25. Periodic boundary condition is used in the span-wise direction in order to reduce the computation costs.

4 RESULTS AND DISCUSSION

4.1 Test chamber description

The test chamber is shown schematically in Fig. 1. It consists of three expansion sections. Section I is 0.266-m long and has a 1° divergence, whereas the corresponding values for Section II are 0.3 m and 3°, and 0.366 m and 4° for Section III. The height of the combustor is 0.0305 m at the entry and 0.07 m at the exit. Two uniform recessed cavities used as flame-holders are located on the upper side wall and the lower side wall in Section I with the distance of 0.115 m to the combustor entry, which makes the test chamber symmetric about the central horizontal plane, and thus only lower half part of the chamber is computed in this work. Liquid kerosene fuel is injected normally into the mainstream from a 0.4-mm diameter orifice, which is located on the cavity ceiling wall 5 mm from the trailing edge. In the numerical study, 5-mm long span-wise section of the combustor is studied, which is equal to the interval space of kerosene injection orifice in experiment by Yu *et al.* [**51**].

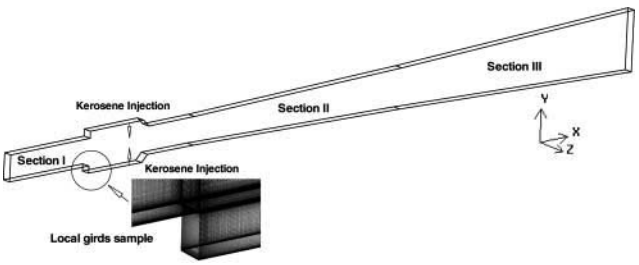

Fig. 1 Sketch of the model supersonic spray combustion chamber and grid sample

In this study, two sets of different cavity lengths are compared, one is 77 mm (Case A) and the other is 45 mm (Case B), and both of them have the same aft-ramp angle of 45° and a depth of 8 mm. The total meshes for LES are approximately 1 million. The domain inside the cavity is discretized using 200 × 80 × 5 cells, and the mainstream region is discretized using 900 × 200 × 5 cells. Grids are clustered towards in the walls and in the shear layer of the cavity. The sample of computational grid is also shown in Fig. 1.

The incoming mainstream of the test chamber has a nominal Mach number of 2.5, whereas its total temperature is of 1720 K and total pressure is of 1.35 MPa. The mainstream's initial species mass fractions of O_2, H_2O, and N_2 are 0.2, 0.134, and 0.666, respectively. Kerosene equivalence ratio is set to be 0.43 in this study.

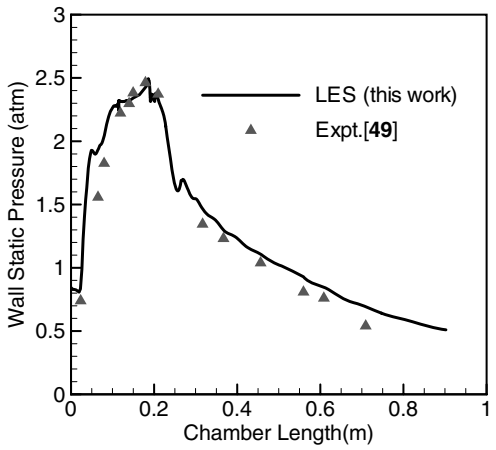

Fig. 2 Pressure distribution from LES of Case A and comparison with experiment

4.2 Statistical characteristics of the flow

The time interval for the statistical process is 2×10^{-7} s. Figure 2 shows the static wall pressure distribution of Case A, compared with the experimental data of Yu *et al.* [**51**]. It can be seen that the overall pressure distribution from LES agrees well with the experimental data. However, due to a lack of accurate inflow boundary layer data to match the experimental condition, small differences between LES and the experimental data are observed near the inlet.

Figure 3 shows contours of the mean temperature, kerosene vapour mass fraction, and combustion intermediate product mass fraction. It can be seen from Fig. 3(a) that there exists a high-temperature zone just above the cavity in the region of shear layer, and temperature inside the cavity is on average 1100 K, which is relatively higher than the chamber inlet temperature (900 K) but nearly the same with the chamber mainstream temperature after the chamber shock waves. Moreover, there is a variation for temperature inside the cavity. The back of the cavity shows on average 1500 K, which is 400 K higher than the cavity front.

Figures 3(b) and (c) show that the kerosene vapour accumulates inside the cavity, especially for kerosene vapour whose mass fraction peaks in the middle of the cavity. In contrast, combustion intermediate products, C_2H_4 in the current case, accumulates in the front corner of the cavity. This shows that kerosene vapour

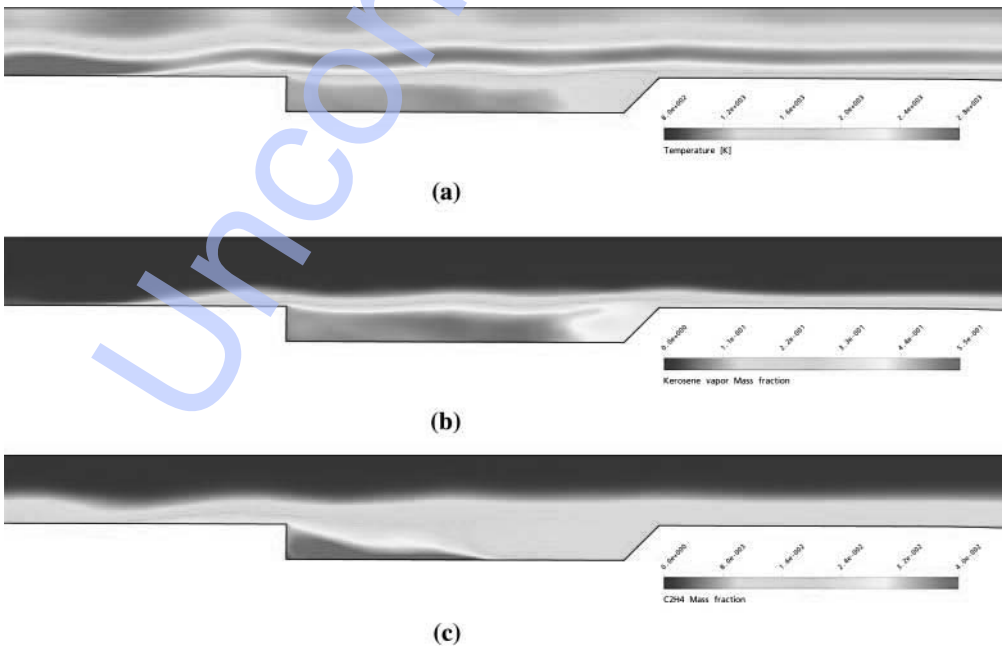

Fig. 3 Contour plots of mean flow quantities: (a) temperature; (b) kerosene vapour; and (c) intermediate product (C_2H_4)

has decomposed during the processes of transporting towards the cavity front inside the cavity.

4.3 Characteristics of the combustion spray

Figure 4 shows the transient liquid cluster trajectory. The droplets are symbolized by small dots with unique diameter, and are coloured by the Sauter Mean Diameter (SMD) distribution. It can be seen that on the ceiling of the cavity, liquid kerosene is injected with uniform velocity through the orifice which has a diameter of 400 μm. Then, the liquid kerosene atomization is modelled by the ETAB model.

Most of the droplets move in the opposite direction to the incoming flow inside the cavity, and very few droplets manage to penetrate through the mixing layer above the cavity into the freestream. In order to make a clear description of the fluid momentum inside the cavity and how it affects the spray momentum, Fig. 5 gives the instantaneous vorticity contour. It can be seen that there is a big recirculation zone near the kerosene spray injection point, and the vortex is full of the whole cavity. Referred to the droplets momentum in Fig. 4, it hints that most of the droplets in the sprays are carried by the recirculation fluid upstream inside the cavity.

Q4

Figure 6 gives detailed information on spray velocity, droplet diameter distribution, and droplet temperature distribution. According to the gas–liquid control equations, the droplets and gaseous phase are coupled through inter-phase sources terms $\tilde{S}_{ui}$, $\tilde{S}_m$, and $\tilde{S}_h$. The inter-phase momentum source represents the force applied on the droplets, and the evaporation processes can be characterized through the inter-phase mass and energy source distribution, as shown in Fig. 7.

It can be seen from Fig. 6 that very few droplets penetrate outside the cavity and are accelerated by the freestream with a relatively higher split speed,

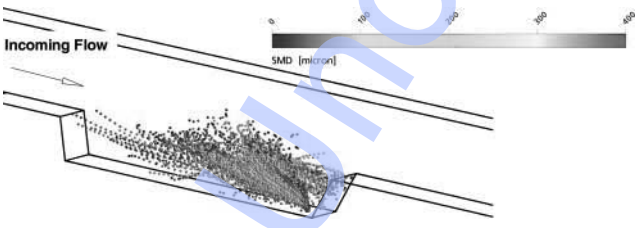

Fig. 4 Liquid kerosene trajectory and droplets coloured by SMD distribution

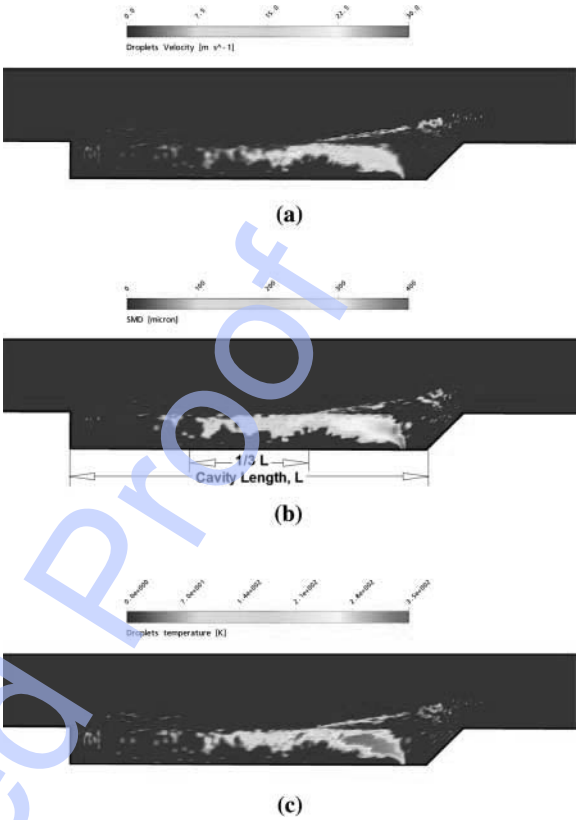

Fig. 6 Contours of droplet quantities: (a) velocity distribution; (b) SMD distribution; and (c) temperature distribution

whereas most of the droplets are loaded by the recirculation fluid motion inside the cavity from the rear wall upstream with a velocity of 8 m/s. The incoming flow velocity is more than 1000 m/s and the average mean velocity for fluid inside the cavity is 30 m/s. During the transportation of the spray, liquid droplets subject to drag from surrounded fluid, resulting in momentum interchange between the spray and the carrier fluid, as shown in Fig. 7 for all source terms. The momentum interchange mainly takes place at the back of the cavity, holding more than one-third of the cavity length (Fig. 7(a)). As a result, droplets break up quickly. Change of SMD from 400 to 100 μm take place within the last one-third length of the cavity, whereas SMD changes from 100 to 10 μm in the middle of the cavity, and droplet diameters nearly disappear at the front of the cavity. Additionally, due to the low velocity of the droplets, sufficient heat interchange takes place between the droplets and the

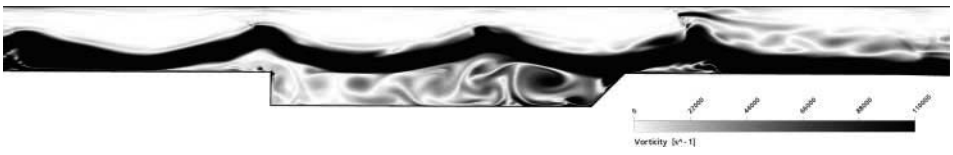

Fig. 5 Instantaneous snapshot of vorticity magnitude

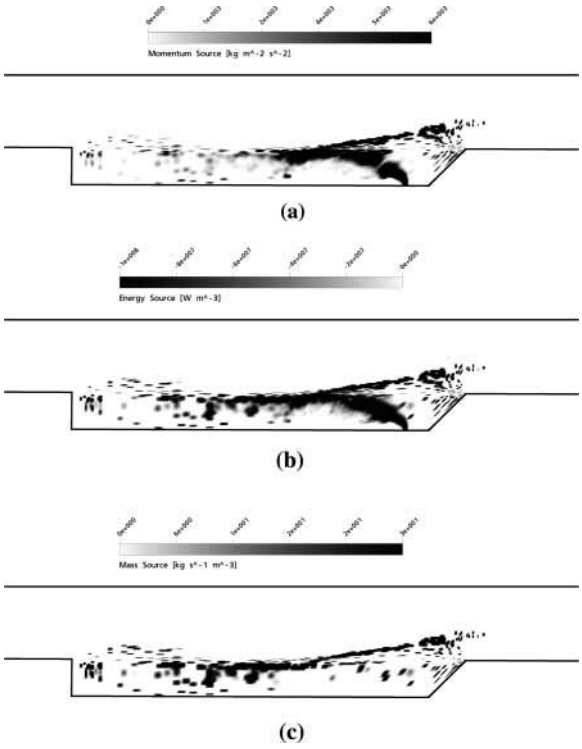

Fig. 7 Distribution of source terms: (a) momentum source; (b) energy source; and (c) mass source

carrier fluid in the whole processes of droplet movement (Fig. 7(b)). Furthermore, it can be seen from Fig. 6(c) that the droplet temperature tends to increase after injection due to absorbing heat from the carrier fluid, whereas the droplet temperature deceases after spray passing through the middle of the cavity caused by evaporation heat consumption. Under the combined effects of atomization and heat interchange, the mass interchange mainly takes place after spray passing through the middle of the cavity (Fig. 7(c)).

It should be noted that, in this test case, a small amount of droplets penetrate out of the cavity during the transportation processes inside the cavity and are reversed back with the mainstream as the results of the shear layer mixing, thus subject to more intensive inter-phase source interchange. However, due to the fact that major inter-phase interchange takes place inside the cavity, these small amount of droplets has no important role in the kerosene vapour generation. Q2

4.4 Characteristics of the instantaneous flow field

Figure 8 gives the instantaneous temperature contour and kerosene vapour distribution at subsequent time instances. Figure 9 gives the typical reaction product

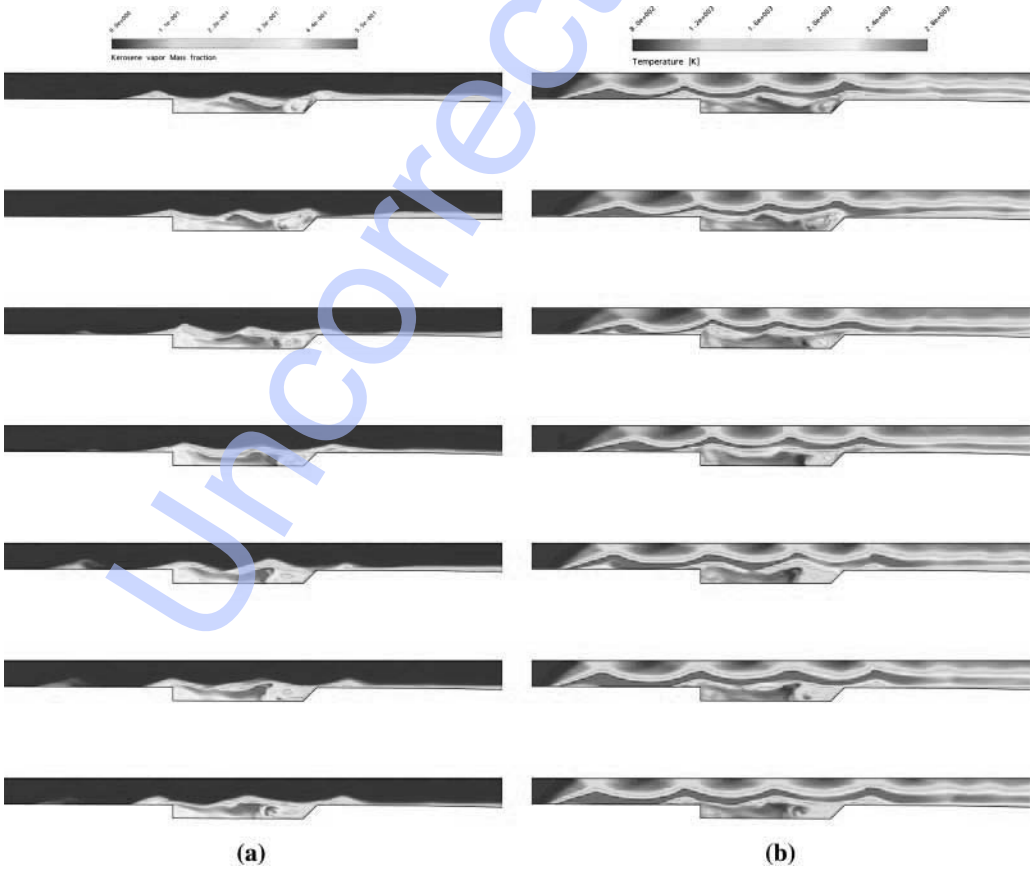

Fig. 8 Time sequence of instantaneous flow field given at equal time interval of 0.08 ms: (a) kerosene vapour mass fraction distribution and (b) temperature distribution

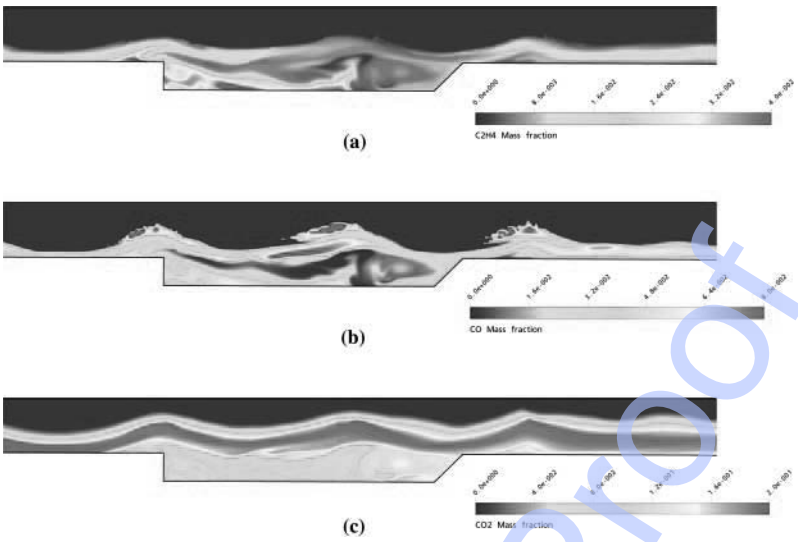

Fig. 9 Typical combustion product distribution for Case A: (a) C_2H_4; (b) CO; and (c) CO_2

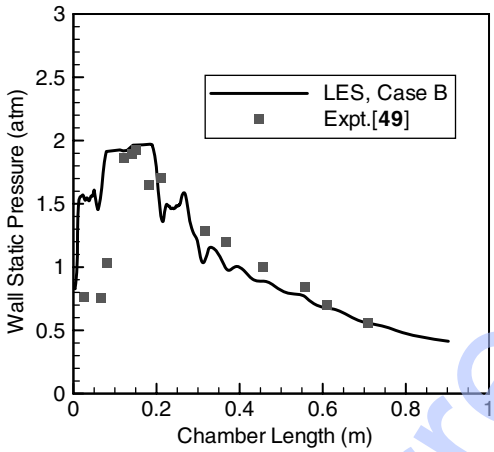

Fig. 10 Pressure distribution of the short length cavity test case

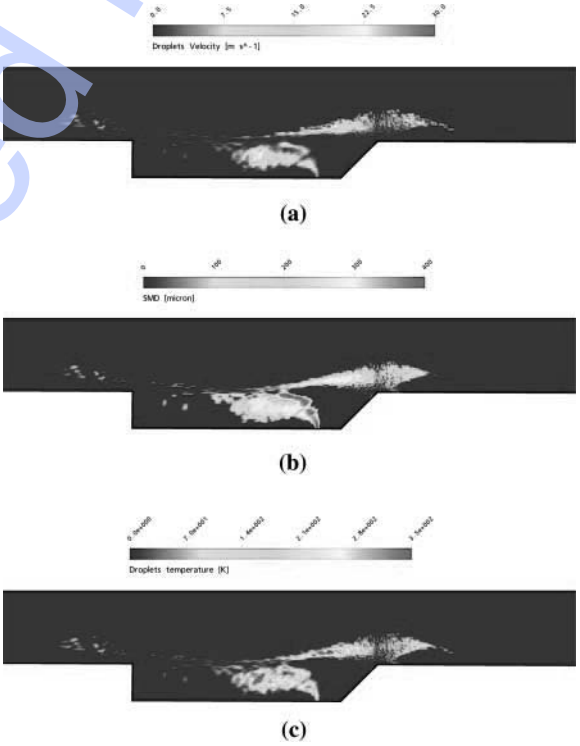

Fig. 12 Contours of the spray droplets: (a) velocity distribution; (b) SMD distribution; and (c) temperature distribution

distribution, including kerosene decomposition product (C_2H_4), combustion intermediate product (CO), and final combustion product (CO_2). It can be seen that the maximum kerosene vapour mass fraction is generated in the middle of the cavity, and only small amount of kerosene vapour spill out of the cavity at the leading edge. The distribution of kerosene vapour is supported by the analysis of spray clusters given above. Moreover, kerosene decomposition takes place during the transportation of the kerosene vapour towards the cavity leading edge, and as a result C_2H_4 mass fraction, shown in Fig. 9, reaches maximum near the cavity front wall. Further oxidation takes place in the approaching boundary layer with air after the resulting C_2H_4 is rolled out of the cavity by the inside vortex, so CO is

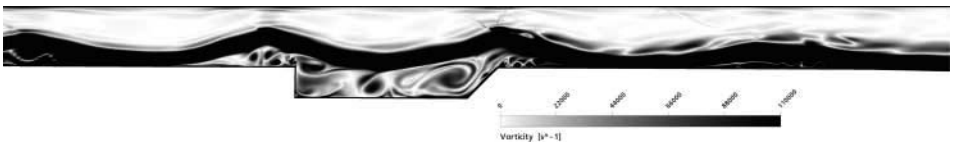

Fig. 11 Snapshot of vorticity magnitude for Case B

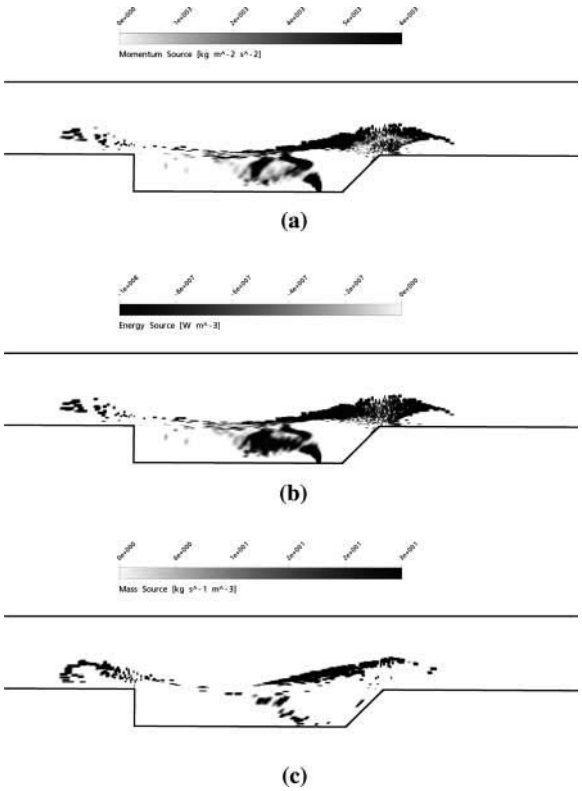

Fig. 13 Contours of droplets source terms: (a) momentum source; (b) energy source; and (c) mass source

mainly generated in the shear layer. Finally, the final combustion product CO_2 is distributed in the whole shear layer covering the cavity.

Temperature inside the cavity is relatively lower, especially in the middle of the cavity due to heat consumption during evaporation and kerosene decomposition. There is also temperature variance inside the cavity, and it can be seen that around the rear wall of the cavity, due to shear layer, hot fluid could impinge the cavity backside wall, and then be reversed back to cavity front, cavity backside shows relatively higher temperature than the cavity front. Furthermore, high temperature in the shear layer can also extend boundary layer separation towards the chamber inlet.

4.5 The influence of cavity length

To study the effect of cavity length on the combustion simulation, another cavity with a length of 45 mm is also performed. All flow conditions are the same as in Case A. Q2

Figure 10 shows the static pressure along the cavity wall. Experimental data of Yu *et al.* [**51**] with the same cavity length are also plotted for comparison. Good agreement is achieved for the later stage in the combustion chamber, and differences between 0 and 0.15 are due to SGS model of LES has the shortcoming to capture the detailed flow structure of the boundary layer separation. Peak combustion pressure for this case is lower than that in Case A (referred to Fig. 2). Figures 11 to 14 give the fluid structure and spray distribution, which can be compared with corresponding figures for the long length cavity, given in Figs 5 to 7 and 9. It can be seen that reducing the cavity length causes more droplets spill out of the cavity, and considerable quantity of evaporation takes place in the shear layer of the cavity. The mass interchange mainly take place in the shear layer outside the cavity, which results in higher C_2H_4 distributing both inside the cavity front wall and near the shear layer around the cavity back (Fig. 14(a)). However, CO_2 mass fraction distribution is lower than that in Case A.

Combustion efficiency, which is defined based on the generation rate of CO_2 at any given vertical panel in chamber, is used here to evaluate the combustion

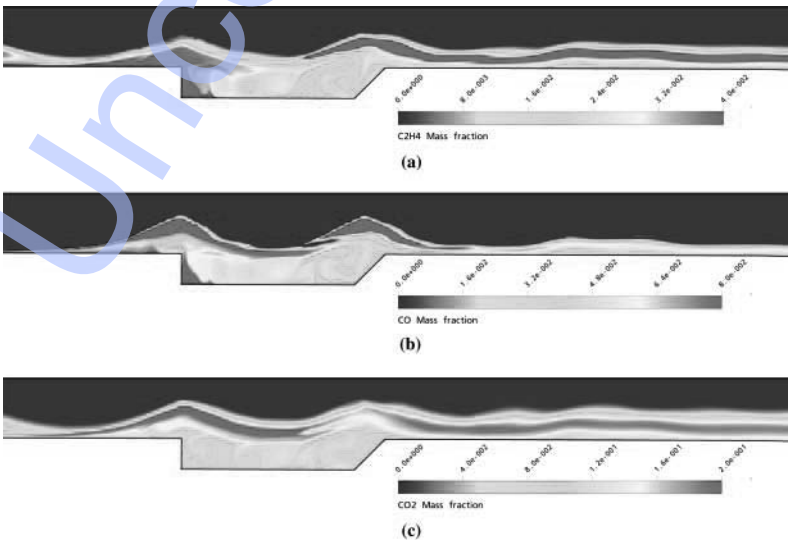

Fig. 14 Typical combustion product distribution of Case B: (a) C_2H_4; (b) CO; and (c) CO_2

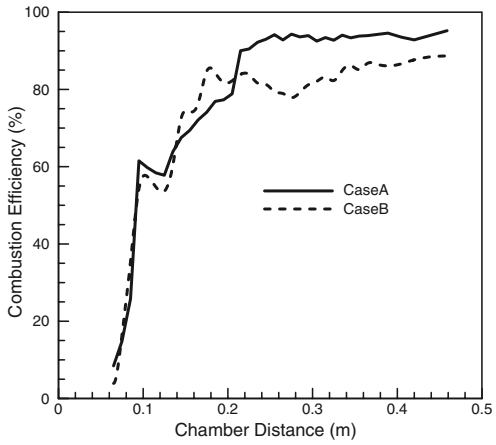

Fig. 15 Comparison of the combustion efficiency along the chamber

performance. Combustion efficiency on a given vertical panel is defined as

$$\eta_c = \frac{\int \rho Y_{CO_2} u \, dA}{\dot{m}_{CO_2,sto}}$$

where $\dot{m}_{CO_2,sto}$ is the mass flowrate of CO_2 corresponding to the overall kerosene fuel combustion under stoichiometric conditions. Figure 15 gives the combustion efficiency distribution along the chamber for all test cases. The combustion efficiency of Case A is higher than that of Case B after the cavity location in the chamber. As discussed above, in Case A, due to sufficient evaporation already taking place inside the cavity, kerosene vapour and kerosene decomposition product are full of the cavity inside, thus these fuel mixtures are rolling with the cavity inner vortex and mixing with the fresh air in the approach mixing layer at the front of the cavity, then are involved into burning in the cavity shear layer. But in Case B, as the reason of parts of droplets spilling out of the cavity, some evaporation takes place in the cavity rear wall shear layer, the evaporated kerosene vapour need distance to get fully mix after the location of cavity, thus resulting in worse combustion performance. The comparison of cavity length shows that fluid structure inside the cavity plays an important role in the spray distribution and further will decide the combustion performance.

5 CONCLUSION

LES of kerosene spray combustion in a model supersonic combustor with cavity flame-holder is carried out. In the test case, kerosene is injected through orifice located in the ceiling of the cavity, and two length scales of cavity are compared in numerical simulation. One cavity length is of 77 mm and marked as Case A, the other is of 45 mm and marked as Case B. Both these cavities have the same after rear angle of 45° and the same depth of 8 mm. In the numerical approach, SGS stress tensor is closed via Smagorinsky's eddy-viscosity model, chemical source term is modelled by FRC model, and four-step reduced kerosene combustion kinetic mechanism is adopted. Chamber wall pressure predicted from LES is validated by previously reported experimental data. In Case A, after liquid kerosene injected through orifice, most of the droplets are loaded with recirculation fluid momentum inside the cavity. Due to lower velocity of carrier fluid inside the cavity, sufficient atomization and evaporation take place during the processes of droplet transportation, resulting in low temperature and rich fuel mixture of kerosene vapour accumulating around the middle of the cavity. These rich fuel mixtures are rolling with the cavity inner vortex and mixing with the fresh air in the approach mixing layer at the front of the cavity, thus are involved into burning accompanied with the approach boundary layer separation extending towards upstream. The combustion flame in the downstream impinges the rear wall of cavity and is then reversed back to cavity front. During the recirculation of hot flow, heat is compensated for evaporation of the droplets. The circulation processes mentioned above provide an efficient flame-holding mechanism to stabilize the flame. In Case B, due to insufficient atomization and evaporation of droplets in the short distance inside the cavity, parts of the droplets are carried out of the cavity through the boundary layer fluctuation and evaporated in the hot flame layer, thus resulting in incomplete air fuel mixing and worse combustion performance. Results of spray combustion with different cavity length scales show that the fluid structure inside the cavity play an important role in the spray distribution, thus determining the combustion performance.

REFERENCES

1 **Heiser, W. H., Pratt, D. T., Daley, D. H.,** and **Mehta, U. B.** *Hypersonic airbreathing propulsion*, 1994 (AIAA). Q5
2 **Cockrell, C. E., Auslender, A. H., Guy, R. W., McClinton, C. R.,** and **Welch, S. S.** Technology roadmap for dual-mode scramjet propulsion to support space-access vision vehicle development. AIAA paper 2002-5188, 2002.
3 **Marshal, L. A., Bahm, C.,** and **Corpening, G. P.** Overview with results and lessons learned of the X-43A Mach 10 flight. AIAA paper 2005-3336, 2005.
4 **Fry, R.** A century of ramjet propulsion technology evolution. *J. Propuls. Power*, 2004, **20**(1), 27–58.
5 **Waltrup, J. P.** Upper bounds on the flight speed of hydrocarbon-fueled scramjet-powered vehicles. *J. Propuls. Power*, 2001, **17**(6), 1199–1204.
6 **Kuo, K. K.** *Principles of combustion*, 2nd edition, 2005 (Wiley). Q5
7 **Stiesch, G.** *Modeling engine spray and combustion processes*, 2003 (Birkhäuser). Q5

8 **Rosener, D. E.** *Transport processes in chemically reacting flow systems*, 2000 (Butterworth).

9 **Luo, K. H.** DNS and LES of turbulence–combustion interactions. In *Modern simulation strategies for turbulent flow* (Eds B. J. Geurts and R. T. Edwards), 2001, pp. 263–295.

10 **Lefebvre, A. H.** *Atomization and sprays*, 1989 (CRC Press).

11 **Blazek, J.** *Computational fluid dynamics: principles and applications*, 2nd edition, 2005 (Elsevier).

12 **Wilcox, D. C.** *Turbulence modeling for CFD*, 3rd edition, 2006 (DCW Industries).

13 **Oran, E. S.** and **Boris, J. P.** *Numerical simulation of reactive flow*, 2nd edition, 2000 (Cambridge University Press).

14 **Baurle, R. A.** Modeling of high speed reacting flows: established practices and future challenges. AIAA paper 2004-0267, 2004.

15 **Fureby, C.** Toward the use of large eddy simulation in engineering. *Prog. Aerospace Sci.*, 2008, **44**(6), 381–396.

16 **Pitsch, H., Desjardins, O., Balarac, G.,** and **Ihme, M.** Large eddy simulation of turbulent reacting flow. *Prog. Aerospace Sci.*, 2008, **44**(6), 466–478.

17 **Janicka, J.** and **Sadiki, A.** Large eddy simulation of turbulent combustion systems. *Proc. Combus. Inst.*, 2005, **30**(1), 37–547.

18 **Vervisch, L., Hauguel, R., Domingo, P.,** and **Rullaud, M.** Three facets of turbulent combustion modeling: DNS of premixed V-flame, LES of lifted nonpremixed flame and RANS of jet-flame. *J. Turbul.*, 2004, **5**(1), 4(1)–4(36).

19 **Veynante, D.** and **Vervisch, L.** Turbulent combustion modeling. *Progr. Energy Combus. Sci.*, 2002, **28**(3), 193–266.

20 **Pael, N.** and **Menon, S.** Subgrid modeling for simulation of spray combustion in large-scale combustors. *J. Propuls. Power*, 2006, **44**(4), 709–723.

21 **Pael, N., Kirtas, M., Sankaran, V.,** and **Menon, S.** Simulation of spray combustion in a lean-direct injection combustor. *Proc. Combus. Inst.*, 2007, **31**(2), 2327–2334.

22 **Pael, N.** and **Menon, S.** Simulation of spray–turbulence–flame interactions in a lean direct injection combustor. *Combust. Flame*, 2008, **153**(1–2), 228–257.

23 **Genin, F.** and **Menon, S.** LES of supersonic combustion of hydrocarbon spray in a SCRAMJET. AIAA paper 2004-4132, 2004.

24 **Gicquel, L. Y. M., Staffelbach, M. G., Cuenot, B.,** and **Poinsot, T.** Large eddy simulations of turbulent reacting flows in real burners: the status and challenges. *J. Phys.: Conf. Ser.*, 2008, **125**(1).

25 **Menon, S., Sankaran, V.,** and **Stone, C.** Subgrid combustion modeling for the next generation national combustion code. NASA/CR-2003-212202.

26 **Pitsch, H.** Unsteady flamelet modeling of differential diffusion in turbulent jet diffusion flames. *Combust. Flame*, 2000, **123**(3), 358–374.

27 **Sankaran, V.** and **Menon, S.** Subgrid combustion modeling of 3-D premixed flames in the thin-reaction-zone regime. *Proc. Combus. Inst.*, 2005, **30**(1), 575–582.

28 **Givi, P.** Filtered density function for subgrid scale modeling of turbulent combustion. *AIAA J.*, 2006, **44**(1), 16–23.

29 **Fureby, C.** Comparison of flamelet and finite rate chemistry LES for premixed turbulent combustion. AIAA paper 2007-1413, 2007.

30 **Norris, J. W.** and **Edwards, J. R.** Large-eddy simulation of high-speed turbulent diffusion flames with detailed chemistry. AIAA paper 97-0370, 1997.

31 **Sun, M., Wang, Z., Liang, J.,** and **Geng, H.** Flame characteristics in supersonic combustor with hydrogen injection upstream of cavity flameholder. *J. Propuls. Power*, 2008, **24**(4), 688–696.

32 **Dagaut, P.** and **Cathonnet, M.** The ignition, oxidation, and combustion of kerosene: a review of experimental and kinetic modeling. *Progr. Energy Combus. Sci.*, 2006, **32**(1), 48–92.

33 **Stiesch, G.** *Modeling engine spray and combustion processes*, 2003 (Birkhäuser).

34 **Schiller, L.** and **Naumann, A.** A drag coefficient correlation. *VDI Zeits.*, 1933, **77**, 318–320.

35 **Bardina, J. E., Huang, P. G.,** and **Coakley, T. J.** Turbulence modeling validation. AIAA paper 97-2121, 1997.

36 **Davidson, P. A.** *Turbulence: an introduction for scientists and engineers*, 2004 (Oxford University Press).

37 **Pope, S. B.** *Turbulent flows*, 2000 (Cambridge University Press).

38 **Hucknall, D. J.** *Chemistry of hydrocarbon combustion*, 1985 (Chapman & Hall).

39 **Westbrook, C. K.** and **Dryer, F. L.** Chemical kinetic modeling of hydrocarbon combustion. *Progr. Energy Combus. Sci.*, 1984, **10**(1), 1–57.

40 **Hautman, D. J., Dryer, F. L., Schug, K. P.,** and **Glassman, I.** A multiple-step overall kinetic mechanism for the oxidation of hydrocarbons. *Combust. Sci. Technol.*, 1981, **25**(5), 219–235.

41 **Gerasimov, G. Y.** and **Losev, S. A.** Kinetic models of combustion of kerosene and its components. *J. Engng Phys. Thermophys.*, 2005, **78**(6), 14–25.

42 **Srlvatsa, S. K.** Computations of soot and NOX emissions from gas turbine combustors. NASA CR-167930, 1982.

43 **Nguyen, H. L.** and **Ying, S. J.** Critical evaluation of jet-a spray combustion using propane chemical kinetics in gas turbine combustion simulated by KIVA-II. AIAA paper 90-2439, 1990.

44 **Lefebvre, A. H.** *Atomization and sprays*, 1989 (CRC Press).

45 **Lefebvre, A. H.** *Gas turbine combustion*, 1998 (Taylor & Francis).

46 **Gosman, A. D.** and **Clerides, D.** Diesel spray modelling: a review. In Proceedings of the ILASS-Europe Annual Meeting, 1997.

47 **Raju, M. S.** Numerical investigation of various atomization models in the modeling of a spray flame. NASA/CR-2005-214033.

48 **Kumaran, K.** and **Babu, V.** Mixing and combustion characteristics of kerosene in a model supersonic combustor. *J. Propuls. Power*, 2009, **25**(3), 583–592.

49 **Tanner, F. X.** Liquid jet atomization and droplet breakup modeling of non-evaporating diesel fuel sprays. *SAE Trans.*, 1997, **106**(3), 127–140.

50 **Yu, G., Li, J. G., Yang, S. R., Yue, L. J., Zhang, X. Y., Huang, Y.,** and **Sung, C. J.** Investigation of liquid hydrocarbon combustion in supersonic flow using effervescent atomization. AIAA paper 02-4279, 2002.

51 **Yu, G., Li, J. G., Chang, X. Y., Chen, L. H.,** and **Sung, C. J.** Investigation of kerosene combustion characteristics with pilot hydrogen in model supersonic combustors. *J. Propuls. Power*, 2001, **17**(6), 1263–1272.